LBL-14578
c.2

Lawrence Berkeley Laboratory

UNIVERSITY OF CALIFORNIA

RECEIVED
LAWRENCE
BERKELEY LABORATORY
JUL 15 1982
LIBRARY AND
DOCUMENTS SECTION

Materials & Molecular Research Division

Presented at the Workshop on Renewable Fuels and Advanced Power Sources for Transportation, Denver, CO, June 17-18, 1982

ENGINEERING ANALYSIS OF AN NH_3- AIR ALKALINE FUEL CELL SYSTEM FOR VEHICULAR APPLICATIONS

P.N. Ross, Jr.

June 1982

TWO-WEEK LOAN COPY

This is a Library Circulating Copy which may be borrowed for two weeks. For a personal retention copy, call Tech. Info. Division, Ext. 6782.

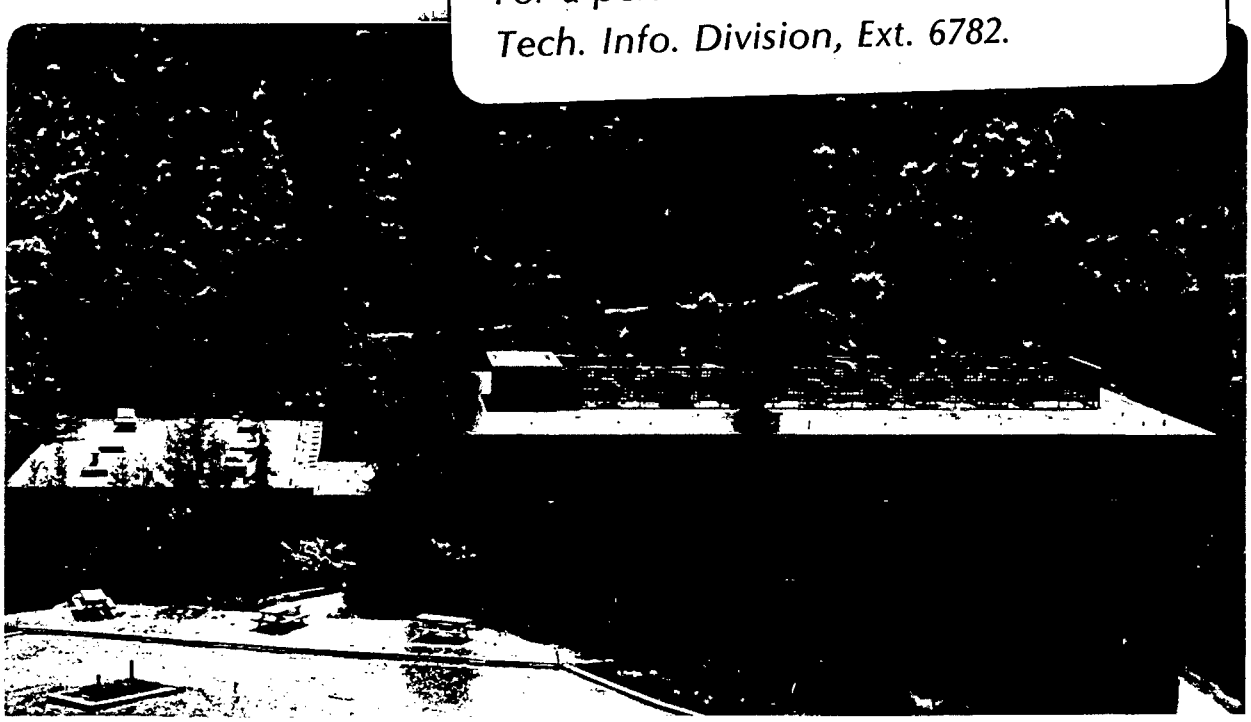

LBL-14578
c.2

Prepared for the U.S. Department of Energy under Contract DE-AC03-76SF00098

DISCLAIMER

This document was prepared as an account of work sponsored by the United States Government. While this document is believed to contain correct information, neither the United States Government nor any agency thereof, nor the Regents of the University of California, nor any of their employees, makes any warranty, express or implied, or assumes any legal responsibility for the accuracy, completeness, or usefulness of any information, apparatus, product, or process disclosed, or represents that its use would not infringe privately owned rights. Reference herein to any specific commercial product, process, or service by its trade name, trademark, manufacturer, or otherwise, does not necessarily constitute or imply its endorsement, recommendation, or favoring by the United States Government or any agency thereof, or the Regents of the University of California. The views and opinions of authors expressed herein do not necessarily state or reflect those of the United States Government or any agency thereof or the Regents of the University of California.

ENGINEERING ANALYSIS OF AN NH_3-AIR ALKALINE FUEL CELL SYSTEM FOR VEHICULAR APPLICATIONS

P. N. Ross, Jr.
University of California
Lawrence Berkeley Laboratory
Materials and Molecular Research Division
Berkeley, California 94720

ABSTRACT

The use of a hydrogen-air alkaline fuel cell in a vehicle with liquid anhydrous ammonia as the hydrogen storage medium was examined. In the system analyzed here, hydrogen is supplied to the fuel cell by the catalytic cracking of liquid anhydrous ammonia, making the total system an indirect NH_3-air fuel cell system. It was found that the endothermicity of the NH_3 cracking reaction can be supplied by combustion of the anode vent gas after utilizing 80% of the hydrogen electrochemically resulting in a minimal efficiency penalty. Laboratory scale examination were made of the ammonia cracking reaction and the power characteristics of an alkaline fuel cell running on cracked ammonia and air. Single cell and bicell testing indicated system thermal efficiencies of 48-60% (based on L.H.V. of NH_3) can be achieved at power densities of 1-2.6 kW/m^2 using currently known electrode technology in a bipolar design. The advantages of the alkaline fuel cell system relative to the methanol-air phosphoric acid fuel cell are higher power density (factor of 2-3) and reasonably good prospects for this maintaining these performance levels with non-precious metal catalysts.

INTRODUCTION

It is well known in the fuel cell field that the kinetics of oxygen reduction are more favorable in alkaline electrolyte than in acid. In the case of supported Pt electrocatalysts, the polarization of a standard fuel cell type gas diffusion electrode is 100-200 mV lower in 35% KOH at 70°C than in 98% H_3PO_4 at 180°C.[1] There are also a number of non-Pt electrocatalysts which have demonstrated at least some promise of providing Pt-equivalent activity for oxygen reduction in alkaline electrolytes.[2,3] Since the early 1960s, there have been a number of technology programs to develop alkaline fuel cells for use in transportation applications. In the U.S. space programs, where cost is not an essential consideration, the NASA-Appolo and Space Shuttle programs have employed alkaline fuel cells with pure (liquified) hydrogen-oxygen very

This manuscript was printed from originals provided by the author.

successfully. The most recent designs have demonstrated truly impressive performances (7.5 kA/m^2 at 0.83V), and energy density (600 Wh/kg) using bipolar stacks with matrix- retained electrolyte.[4] However, attempts to develop alkaline fuel cell technology for terrestial applications have not met with comparable success. An historical review of these efforts was given by Kordesch,[5] where it was shown how major emphasis in fuel cell programs shifted away from alkaline to acid electrolyte systems during the last decade. There are two major reasons for this shift. The first is related to a change in both application and primary fuel, away from transportation and pure hydrogen to stationary power from hydrocarbon fuels. Steam reforming and water-gas shifting of hydrocarbons generates 20-25% CO_2 in the fuel gas and the onsite removel of CO_2 to acceptable levels for strong alkaline electrolyte imposed too large on economic penalty. The second is related to technological problems encountered in attempts to develop lower cost alkaline fuel cell systems.[6] Kordesch[7] has suggested that the principal problem has been high internal resistance in previous cell designs, a problem which can be overcome by developing a bipolar cell design like that developed for phosphoric acid fuel cells (PAFC).[8] In this paper, we report the results of studies on laboratory scale (16 cm^2) bipolar flowing electrolyte cell that used the supported Pt catalyst, the graphite bipolar plates and the carbon-paper electrode substrates from PAFCs with polypropylene separator plates. These studies have shown that one can, in fact, realize the high power density capability of alkaline electrolyte with a cell design of this type.

The use of hydrogen-air fuel cells in vehicles requires the development of a technology for on- board storage of hydrogen. This problem has been examined extensively in recent years, and the literature is too numerous to review here in detail. Work on hydrogen storage in metal hydrides has been reviewed by Reilly, et al.[9] and by Buchner.[10] The technology of liquid hydrogen storage in cryogenic containers is summarized in the survey by Escher.[11] Swisher and Johnson[12] have examined the relative merits of metal hydrides, liquid hydrogen and microcavity[13] storage of hydrogen on vehicles using efficiency, weight, cost and safety as criteria. The conclusion from that comparison was that from both safety and energy efficiency considerations, metal hydrides or microcavity storage is preferred over liquid hydrogen although the latter has superior energy density. The current state-of-the-art in metal hydride storage of hydrogen is only about 2 w/o in hydrogen (e.g. 5.4 kg hydrogen in 340 kg for the Daimler-Benz vehicle[10]), and it has been shown in computer simulation studies that such a heavy storage system is impractical for a fuel cell powered vehicle.[14] Unfortunately, very few studies of hydrogen storage technology include anhydrous liquid ammonia as a chemical storate(in effect, an inorganic, nonmetallic hydride) in spite of the fact that it is 17.6 w/o hydrogen and has a relatively low heat of formation (2.7 kJ/g versus 3.0 kJ/g for MgH_2). One of the few studies which had included ammonia was the advanced vehicle propulsion study at LLNL.[15] Their analysis included all the auxiliary equipment required to store and thermally crack the ammonia (to H_2 and N_2), and showed that the energy density was 2.5 times higher than iron-titanium hydride and 1.8 times higher than magnesium-nickel hydride (about 3.4 w/o hydrogen inclusive of the tank and all components required to deliver hydrogen to the power converter). According to the LLNL study, the principal

disadvantage of ammonia was the potentially adverse effects of undissociated NH_3 on the combustion of the cracked NH_3 in an internal combustion engine (ICE). With a fuel cell power converter, undissociated NH_3 may be much less of a problem.

We report here the examination of an alkaline fuel cell system for vehicles using anhydrous liquid ammonia as the hydrogen storage medium and cracked ammonia as the anode feed to the bipolar fuel cell. The use of ammonia as a hydrogen carrier for fuel cells is not new or unique to this work, and there have been previous efforts to develop cracked ammonia-air alkaline fuel cells for vehicles.[16] Previous work on ammonia systems did not describe in detail the manner in which the endothermic heat of cracking was provided, i.e. system integration, or state the overall system efficiency achieved. In this work, detailed mass and energy balances are described for the fuel cell system and we report laboratory studies of the kinetics of ammonia cracking, the effects of unreacted ammonia on the cell reactions, and the power characteristics of a bipolar fuel cell using supported Pt catalysts. Based on these laboratory evaluations, an ammonia- air fuel cell system design for a vehicle powerplant was developed and used in a computer simulation for passenger vehicles that is described elsewhere.[17]

SYSTEM INTEGRATION

The components, material flows and temperatures are shown in Fig. 1. Detailed specifications of key components of the systems are given in a subsequent section. Ammonia is stored as a saturated liquid in a pressurized tank designed for a maximum operating pressure of 20 bar. The ammonia is vaporized in this tank using the waste heat from the fuel cell, superheated by the cracked product and fed to the reactor for hydrogen generation. The steady-state operating condition for the converter is ca. 10 bar and 450°C using a standard ammonia synthesis catalyst. The equilibrium conversion of ammonia to hydrogen and nitrogen can be calculated from the experimental values of the equilibrium constants tabulated by Larson and Dodge.[18] We define K_p for the reaction as written

$$2NH_3 \rightarrow N_2 + 3H_2$$

$$K_p = \left[P_{N_2}\, P_{H_2}{}^3/P_{NH_3}{}^2\right]^{1/2} = P\left[X_{N_2}\, X_{H_2}^3/X_{NH_3}^2\right]^{1/2} \qquad [1]$$

$$= P\, K_x \text{ or } K_x = K_p/P$$

where X_i are the mole fractions and P is the total pressure. The equilibrium conversion, η, is related to K_x by

$$\eta = \sqrt{\frac{K_x}{0.918+K_x}} \qquad [2]$$

Increasing temperature increases the conversion, as the reaction as written is endothermic, and increasing pressure decreases conversion as

shown in Table 1. Pressure, however, has a very favorable effect on the kinetics and on reactor volume and mass. For maximum system efficiency, the cracker temperature should be the minimum required to achieve conversions approaching unity. The relationship between the equilibrium conversion (cracking temperature and pressure) and both system efficiency and weight was examined in considerable detail, as discussed in a later section. If unreacted ammonia is assumed to have no adverse effect downstream, then the optimum condition for cracking is 450°C at 10 bar. The cracker is therefore designed to operate nearly isothermally producing cracked ammonia at the equilibrium conversion of 0.971. The composition of the gas leaving the cracker is, therefore, 1.5% NH_3, 73.9% H_2. The product gas is cooled by heat exchange with the ammonia feed and expanded to ambient pressure before entering the fuel cell.

It is not possible to state definitively in what streams and at what concentrations unconverted ammonia leaves the system. At 80°C, ammonia has a very low solubility in water (<1 g/ℓ) and the estimated rate of crossover of ammonia from the anode to the cathode is 10^{-8} moles cm^{-2} sec^{-1}. At current densities of 2-4 kA/m2 with 2.5 times stoichiometric air, the estimated concentration of ammonia in the cathode exhaust is therefore 100 ppm. Most of the unconverted ammonia passes directly through the fuel cell and is combusted in the burner to <1 ppm emission in the burner exhaust.

The fuel cell is of the flowing electrolyte type, with a steady-state operating condition of 80°C using 35% KOH electrolyte. Hydrogen is converted at the anode via the half-reaction

$$2H_2 + 4\ OH^- \rightarrow 4\ H_2O + 4e^-$$

Oxygen is consumed at the cathode in the half-reaction

$$O_2 + 2H_2O + 4e^- \rightarrow 4\ OH^-$$

The half-reactions clearly indicate the gradient in H_2O concentration that will develop in an operating cell. The anode gas enters the cell completely dry, and water produced in the gas diffusion electrode is transported both by evaporation to the anode effluent and by liquid phase diffusion into the bulk electrolyte. The water transport processes and a calculated water balance around the cell is shown in Fig. 2. The relative amounts of water carried out by the anode and cathode exhaust streams will depend on the convective transport of water in the flow electrolyte, the transpiration rate of water from the air cathode and the degree of saturation of air in the CO_2 scrubber. Detailed modelling of these transport processes was beyond the scope of the present study. The water balance shown in Fig. 2 is based on the following assumptions: i) the electrolyte in the cell is nearly perfectly mixed at 35% KOH; ii) the anode gas becomes saturated with water at equilibrium with 35% KOH at 80° C; iii) the balance of the product water leaves the cell via the product water carried out by the electrolyte. The water balance for Fig. 2 is for process air that is 2.5 times the stoichiometric amount, which is sufficient flowrate to carry out all product water without saturation of the cathode gas, i.e. there is excess water carrying capacity in the process air stream at 2.5 times stoichiometric air flow.

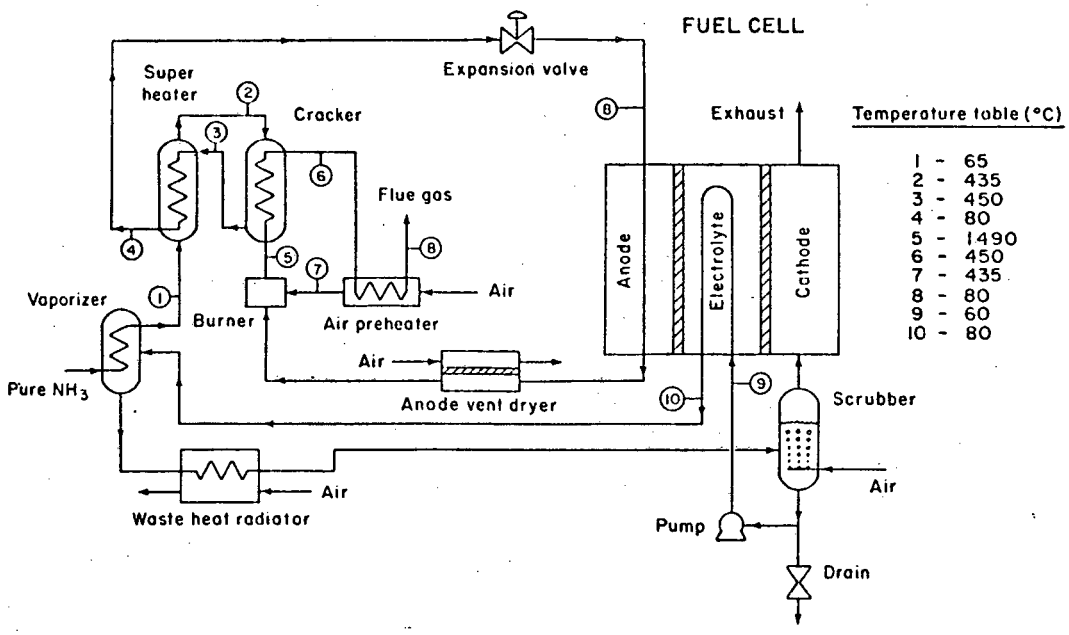

FIG. 1. SCHEMATIC DIAGRAM OF THE THERMALLY INTEGRATED NH_3-AIR FUEL CELL SYSTEM.

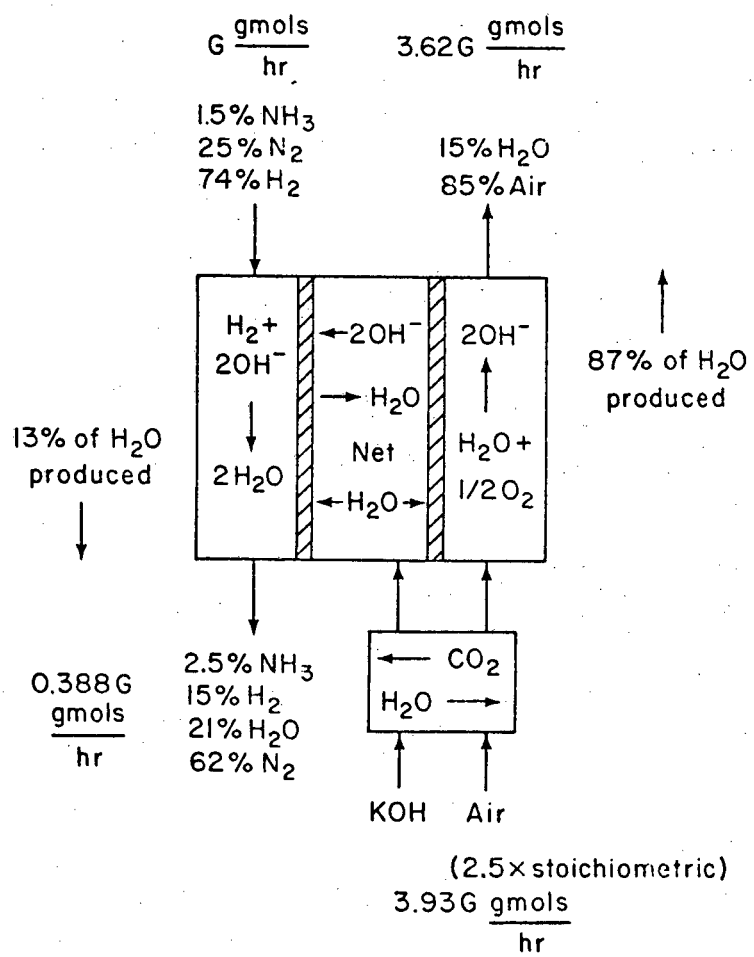

FIG. 2. CALCULATED WATER BALANCE AROUND THE ALKALINE FUEL CELL AT STEADY-STATE.

As shown in both Figs. 1 and 2, process air is scrubbed of carbon dioxide using the recirculating electrolyte in a two-phase contactor. The contactor also serves to fine tune the water balance on the fuel cell since excess product water carried out of the cell by the electrolyte would be evaporated in the contactor. $KHCO_3$ has sufficient solubility[19] in water at the operating temperature of the fuel cell (ca. 180 g CO_2 per liter 35% KOH at 60-80°C) that approximately 500 kWh of energy can be extracted before carbonate insolubility becomes a problem. This design, therefore, calls for complete replacement of the electrolyte (e.g. 2.5 ℓ for a 20 kW fuel cell) every 500 kWh, or about every 5000 km for a 4-passenger vehicle. Longer service intervals for the electrolyte are possible by the use of soda pre-scrubbers that take 90% of the carbon dioxide out of the process air; the soda scrubber can be disposable or can be regenerated using waste heat from the ammonia cracker.

The cracking of ammonia to nitrogen and hydrogen is endothermic and requires a continuous input of enthalpy. In steady-state operation, this enthalpy is supplied entirely by combustion of unreacted hydrogen from the fuel cell anode effluent. The detailed energy balance indicated that if 80% of the hydrogen produced by cracking ammonia is consumed electrochemically in the fuel cell, combustion of the balance of the hydrogen with stoichiometric air provides the required heat of reaction in the cracker. The adiabatic flame temperature for complete combustion of the dehumidified anode effluent with stoichiometric air is 1490°C and the total enthalpy exchanged with the cracker at 450°C (i.e. burner gas ΔT = 1040°C) is 54.8 kJ per gmol ammonia feed, which is slightly larger than the enthalpy requirement of the cracking reaction (51.7 kJ) at 97.1% NH_3 conversion. In order to supply the enthalpy of cracking at 450°C with just 20% of the hydrogen, it is necessary to dry the anode vent gas to maximize the adiabatic flame temperature. This is done with a membrane dehumidifier which exchanges water vapor with the ambient air.

For cold-starting the system, the heat required to start the ammonia cracker is supplied by the combustion of a hydrocarbon fuel (e.g. liquified propane). Although ammonia itself could be burned to supply this heat, a hydrocarbon fuel is a better choice for this specific purpose, as the higher enthalpy of combustion reduces the quantity of fuel required. Cold start will often require a higher reaction temperature in the cracker than the steady-state operating temperature of 450°C. Since the ammonia storage is essentially at ambient temperature in a cold start condition, very cold ambient (<0°C) would reduce the delivery pressure of ammonia to the cracker well below 10 bar. To achieve high conversion in the cracker at reduced pressure, the reaction temperature must be greater than 450°C, e.g. 550°C for >97% conversion at 1 bar. At 25°C, the alkaline fuel cell can deliver energy at about one-half the design power density, and the system has self-starting capability, i.e. waste heat from the fuel cell heats the electrolyte and the stored liquid ammonia up to the steady-state operating temperature. The actual start-up time for this system is not known; from heat transfer calculations the estimated start-up time from 25°C is 200 seconds.

A summary of the system energy characteristics showing the achieved balance between endothermic and exothermic processes is given in Table 2. All product water is vaporized to maintain an invarient (weight and

TABLE 1. EFFECT OF TEMPERATURE AND PRESSURE ON THE EQUILIBRIUM CONVERSION OF AMMONIA TO NITROGEN AND HYDROGEN.

Effect of Temperature on Equilibrium

T (°C)	K_p	η(%) 10 bar	η(%) 1 bar
550	440	99.0	99.9
450	151	97.1	99.8
350	36.5	90.6	98.8
300	14.6	78.4	97.0

Effect of Pressure on Equilibrium

Pressure (bar)	K_p	K_x	η(%)
1	150.60	150.60	99.8
10	151.75	15.18	97.1
30	147.93	4.93	91.8
50	144.93	2.90	87.2
100	137.95	1.38	77.5
300	113.12	0.38	54.1
600	77.28	0.13	35.2
1000	42.96	0.04	20.4

TABLE 2. ENERGY BALANCE SUMMARY (BASIS: 1g mole NH_3)

Endothermic Processes		Exothermic Processes	
Heat for NH_3 Cracking	51.7 kJ	Heat from combustion of anode vent gas	54.8 kJ
Sensible Heat Losses	728 J		
Heat for Vaporization of Product H_2O	52.9 kJ	Waste Heat from Fuel Cell	$\frac{101.6 \text{ kJ}}{V^*}$
Heat for Vaporization of NH_3	22.9 kJ		

*V is volts per cell in the fuel cell.

volume) electrolyte, and at the design operating voltages of 0.7-0.8 V per cell the excess enthalpy of reaction in the cell provides sufficient energy to evaporate the product water and the ammonia feed. The net electrical energy delivered by the system per gmol of ammonia feed is given by Faraday's Law,

$$E = 3F\ \eta\ UV \qquad [3]$$

where F is the Faraday constant, η is the fractional conversion of NH_3 in the cracker, U is the fractional conversion of hydrogen in the fuel cell and V is the cell voltage. Since the system produces water vapor as opposed to liquid water, we compute the system thermal efficiency based on the lower heating value of liquid ammonia (LHV), defined as the standard enthalpy of the reaction as written

$$NH_3\ (\ell) + \frac{1}{2} O_2(g) \rightarrow N_2(g) + H_2O(g) \qquad [4]$$

which is -295.4 kJ/gmol using the thermochemical data of Rossini.[26] Then the system thermal efficiency is given by

$$\varepsilon = 0.9794\ \eta\ UV \qquad [5]$$

The thermal efficienty computed from [5] may be compared directly with the literature values for heat engines as the basis is exactly the same, combustion of liquid fuel to gaseous product. The system of Fig. 1 is designed to operate at η = 0.971 and U = 0.8 with cell voltages of 0.7-0.8V. The system thermal efficiency is, therefore, expected to be 53-61%, or about twice the full-throttle efficiency of internal combustion engines using gasoline.[20] Of greater practical consequence for vehicle use is the net energy delivered by the power source per unit weight (or volume) of fuel, which is the product of the thermal efficiency and the energy density of the fuel, or in this case

$$ED = \begin{cases} 17.02\ \eta\ UV & kJ/g\ NH_3{}^{\dagger} \\ 10{,}245\ \eta\ UV & kJ/\ell\ NH_3 \end{cases} \qquad [6]$$

using 0.602 g/cm^3 as the density of ammonia at the storage conditions here (20 bar, ambient temperature) exclusive of the weight of the fuel tank. For the power source designed here, the energy density would be 8.7-10.6 kJ/g, which is comparable to that for a gasoline- ICE power source (ca. 10kJ/g at full throttle)[20] even though the LHV of ammonia is less than half the value for gasoline. In principle, therefore, this system is at least potentially capable of use as a vehicle power source with range and performance equivalent to contemporary gasoline- ICE powered vehicle but with much higher energy efficiency. The key to practical utilization of this energy conversion system is the power density (weight <u>and</u> volume basis) and the cost of the power plant. The primary emphasis in this study is the determination of the power density possible using lightweight materials like graphite and polypropylene.

† 1 kJ/g equals 0.278 kWh/kg.

LABORATORY STUDIES

Laboratory studies were conducted on the two major components in the system, the ammonia cracker and the alkaline fuel cell.

Ammonia Cracking

As there is both a substantial literature on ammonia decomposition[21] and readily available catalyst technology, the present studies were restricted to the determination of empirical kinetic expressions for a particular commercial catalyst at the conditions of interest. These empirical expressions were then used to calculate the catalyst loading required as a function of operating conditions and will be used in future modelling studies.

The decomposition of ammonia was performed in a flow system at 1 bar with a differential reactor using a pelletized commercial ammonia synthesis catalyst (United Catalysts doubly promoted iron). The catalyst was prereduced in flowing hydrogen at 600°C. Mixtures of ammonia and hydrogen with helium as diluent were passed over the catalysts with the total flowrate adjusted to give differential conversion (<10%). The concentration of ammonia in both inlet and outlet streams was measured using a photoionization detector (HNU Systems, Model PI-51), and the reaction rate was calculated from the difference between the in and out flowrates. Reaction orders were determined by varying the ammonia flowrate at constant hydrogen flow and vice versa. A few experiments were done using nitrogen as diluent which confirmed the general conclusion in the literature[21] that the reaction is zero order in nitrogen pressure. The rate data were fit with the Temkin-Pyzhev power law expression[21]

$$r = k\left(P_{NH_3}{}^{m}/P_{H_2}{}^{n}\right)$$

for which the best fit parameters were m = 0.75, n = 0.38 and k = 6.4 x 10^{-2} gmol hr^{-1} g^{-1} at 450°C (Arrhenius temperature coefficient 145 kJ/gmol).

For an isothermal tubular (plug-flow) reactor, the weight of catalyst (W_c) required to achieve a given fractional conversion (η) of ammonia will be given by

$$W_c = Q\int_0^{\eta}\frac{d\xi}{r} = \frac{Q}{k}P^{n-m}\int_0^{\eta}\left(\frac{3\xi}{2+2\xi}\right)^{n}\left(\frac{1-\xi}{1+\xi}\right)^{-m}d\xi \qquad [7]$$

where P is the total pressure (in bars), ξ is the fractional conversion η is the equilibrium conversion and Q is the ammonia feedrate in gmols/hr. It is seen from [ ] that for m = 0.75 and n = 0.38 the pressure dependence of the reactor volume is - 0.38, so that operation of the cracker at 10 bar versus 1 bar reduces the weight of catalyst required by a factor of about 2.5. Examination of the form of the integral as a function of η, shown in Fig. 3, gives a great deal of insight into the kinetic problems associated with equilibrium conversions (η) approaching unity. The inverse pressure dependence of the kinetic rate on hydrogen partial pressure causes the differential rate at high conversion to drop

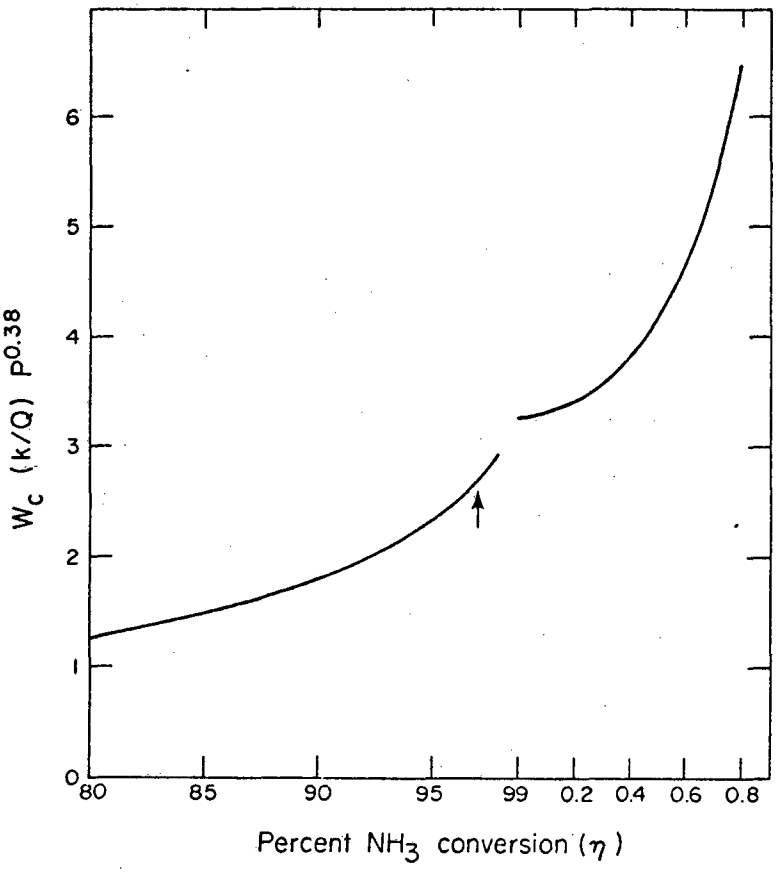

FIG. 3. CATALYST LOADING (W_c) REQUIRED TO ACHIEVE A GIVEN INTEGRAL CONVERSION (η) OF NH_3 TO H_2. ARROW REPRESENTS THE EQUILIBRIUM CONVERSION AT THE STEADY-STATE DESIGN POINT.

by orders of magnitude from the initial rate, i.e. the rate is high at the front of the catalyst bed, very low at the exit. At the design conditions of 450°C and 10 bar, the amount of catalyst required to achieve equilibrium conversion is 1.13 (Q/k). Lowering the pressure to 1 bar would allow equilibrium conversions as high as 99.8 (Table 1) but would require 6.5 (Q/k) grams of catalyst, or nearly six times the amount of catalyst. Equilibrium conversions >99% at 10 bar can also be achieved by raising the cracking temperature from 450°C to 575°C (Table 1). Because of the large temperature coefficient for the rate constant, this higher conversion can be achieved with even less catalyst, but the total system efficiency is reduced because more hydrogen must be burned to increase the adiabatic flame temperature by 125°C. An adiabatic flame temperature of 1625°C instead of the 1500°C required for cracking at 450°C requires combustion of about 25% of the hydrogen versus 20%, i.e. the hydrogen utilization in the fuel cell drops from 80% to 75% and lowers the system efficiency by 4%. There is, therefore, reasonable flexibility in the framework of the present design as to the level of unreacted ammonia in the anode gas stream within the range of 1-3%. However, conversions of ammonia greater than 99% impose unacceptable penalty in either weight (volume) or system efficiency and do not appear practical in vehicle application.

Bipolar Alkaline Fuel Cell

Two laboratory scale hydrogen - air fuel cells were built and tested in this investigation. The first was a single cell built to test the separator and electrolyte flow design and to obtain characteristic performance for the subscale electrodes. The four electrode bicell had all the components of the repeating hardware in a bipolar flowing electrolyte cellstack, e.g. bipolar plates, separators, flow manifolds, and end plates. A diagram of the components is shown in Fig. 4 and the configuration of the laboratory bicell is shown in Fig. 5. Because of the high current densities at which this fuel cell is intended to operate (2-5 kA/m^2), the minimization of ohmic losses in current collection and in electrolyte resistance are essential. Backplane current collection was used with ribbed bipolar graphitic carbon plates in PAFC designs. The graphite bipolar plates and end plates were machined from surface-finished graphite sheet (Union Carbide, Grade ATJS, 0.32 cm thick) and used without further treatment. The separator was machined from a surface-finished sheet of polypropylene (Corth Plastics, 0.28 cm thickness). A reference electrode capillary, not shown in Figs. 4 or 5, was drilled into the lower liquid flow manifold and polytetrafluoroethylene tubing (Dupont PTFE) was used to connect an Hg/HgO reference electrode to each cell. The electrodes were also of the phosphoric acid fuel cell type, consisting of a polytetrafluorethylene (PTFE) bonded catalyst layer on a hydrophobic porous carbon paper susbstrate. The carbon paper (Stackpole PC 206) was first wetproofed using normal PAFC practice, e.g. impregnation with PTFE, either as TFE-30B or FEP 120 (DuPont), nominally 25-30 w/o PTFE solids, with a curing temperature of 350°C. For use in flowing hot 35% KOH electrolyte, it was found that further wetproofing was necessary. This was accomplished by impregnating the wetproofed paper with 2 mg/cm^2 of acetylene black (Shawinigan) - TFE 30B mixture (35 w/o TFE solids) and curing again at 350°C. The active area in these cells was 16 cm^2 (4 x 4) with a 1 cm region on the perimeter of the electrode used for manifolding both gas and liquid. No gaskets or O-rings were used for sealing. Both gas and liquid sealing was accomplished using a PTFE film seal between the separator plate surface and the front or back of the carbon paper substrate. The PTFE was applied by brushing on a concentrated isopropyl alcohol-PTFE (Dupont TFE-3170) slurry and air curing at 120°C. The catalyst used in this work was a commercially available material, 10 w/o Pt supported on Vulcan XC 72 R, purchased in this instance from Prototech. We found that the best air cathode performance was obtained by heat-treating the standard Prototech catalyst.[22] The catalyst layers contained 25 w/o PTFE (DuPont TFE-30B) solids and were applied by direct vacuum filtration of a isopropanol/water suspension directly through the wet-proofed paper. The fabricated electrodes, with the TFE film and catalyst layer were given a final air curing at 320°C.

The graphite end plates, electrodes, separators and bipolar plate were stacked in a filter-press geometry between copper end plates fitted with cartridge-type heaters and thermistor controller (used to bring the stack up to temperature). Electrolyte (35% KOH) was circulated through the cell stack using a PTFE diaphragm metering pump (Cole-Parmer, Model C-7180) through PTFE tubing. The anode gas was simulated cracked ammonia, produced by passing a calibrated 25% N_2/H_2 mixture through a saturator

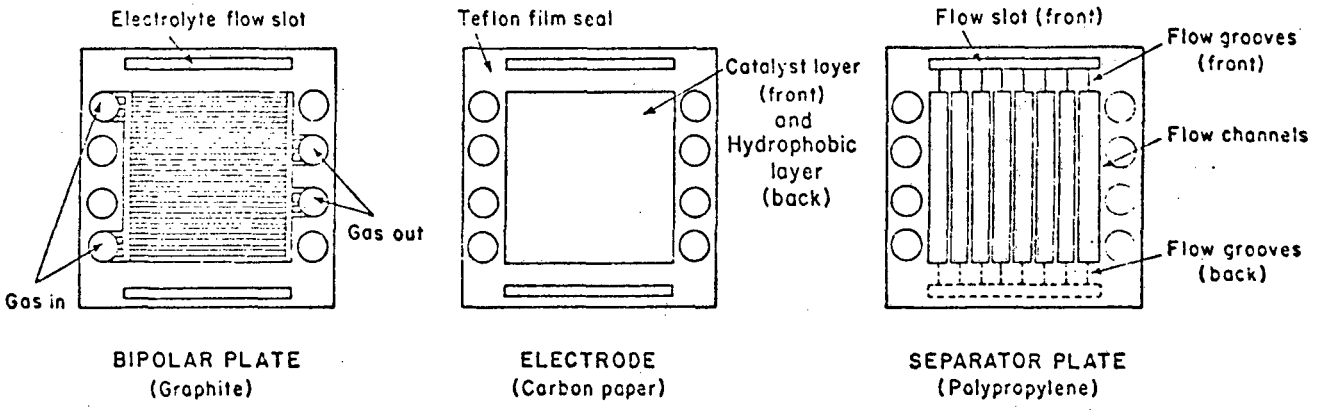

FIG. 4. SCHEMATIC DIAGRAM OF REPEATING COMPONENTS OF THE BIPOLAR FLOWING ELECTROLYTE FUEL CELL.

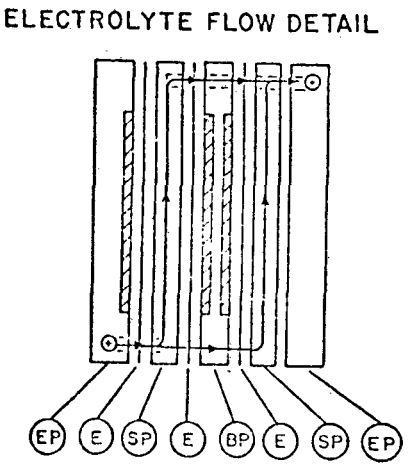

FIG. 5. SCHEMATIC DIAGRAM OF THE LABORATORY BICELL (PARALLEL FLOW).

containing 3.5 w/o NH_3 aqueous solution thermostated at 55°C (NH_3 vapor pressure ca. 13 kPa). The oxidant gas was a 20% O_2/N_2 calibrated mixture that was pre-saturated with water vapor to match the vapor pressure of 35% KOH at 80°C. The gas flowrates were controlled with rotameters calibrated for each stream using positive displacement methods.

The current-voltage behavior of the single cell and bicells was measured using a PAR 371 Potentiostat/Galvanostat as a programmable solid state load. Single electrode potentials were measured against an external Hg/HgO reference electrode and corrected for solution resistance using current interruption by a mercury- wetted relay. The anode gas flow was usually adjusted to correspond to 80% utilization of the hydrogen and the cathode gas to 2.5 the stoichiometric rate of oxygen. For diagnostic purposes, the gas flows were periodically run at essentially zero utilization, and the composition of the gases switched to pure hydrogen and pure oxygen.

The initial polarization behavior of the cells were found to be very dependent on the start-up procedure. The optimum procedure observed was: flow pure oxygen on both electrodes; heat to 80°C at open circuit; stand at open circuit at 80°C for 24 hrs; purge the anode with N_2, switch to pure H_2; sustain a 5 kA/m^2 load at zero utilization for 4 hrs; switch to cracked ammonia and air (20% O_2/N_2) with utilization of gases. After this start-up procedure, relatively invariant polarization behavior was observed, although long-term (>100 hrs) characteristics of the cells were not part of the present study.

The 16 cm^2 single cell performance curve, terminal voltage versus current, is shown in Fig. 6. The measured total cell resistance was 1.25 Ω; the expected solution resistance for the interelectrode gap of 0.28 cm is 1.03 Ω using the conductivity data of Dyson, et al.,[23] so the cell resistance seems to be almost entirely in the solution. One could, therefore, increase the peak power over that in Fig. 6 by reducing the interelectrode gap using a thinner separator. However, the diffusion losses will still limit the peak power even if the cell resistance were reduced to zero. This effect is easily seen in the power curves shown in Fig. 7, which were generated by subtracting the resistance effect due to the reduction in separator thickness from the one used. The peak power can be improved by about 10% by employing a thinner separator, although there appears to be little to gain by reduction below 0.15 cm. In the voltage region of 0.7 - 0.8 V, which is the best voltage for the fuel cell in a vehicle, reduction of the electrode gap from that used here has relatively little effect on the power density at this voltage.

The current voltage characteristics for the four electrode bicell is shown in Fig. 8. The total cell resistance was 2.5 Ω, exactly twice the single cell resistance, indicating the graphite bipolar plate added negligible Ohmic resistance and that current collection was accomplished with very low contact resistance. However, at high current density, the terminal voltage was slightly less than twice the single cell voltage. Individual electrode potentials indicated the problem was in the electrodes themselves, and not intrinsic to the design of the bipolar cell, e.g. shunt currents. In the context of this small laboratory program, we found that it was very difficult to produce four optimum performance

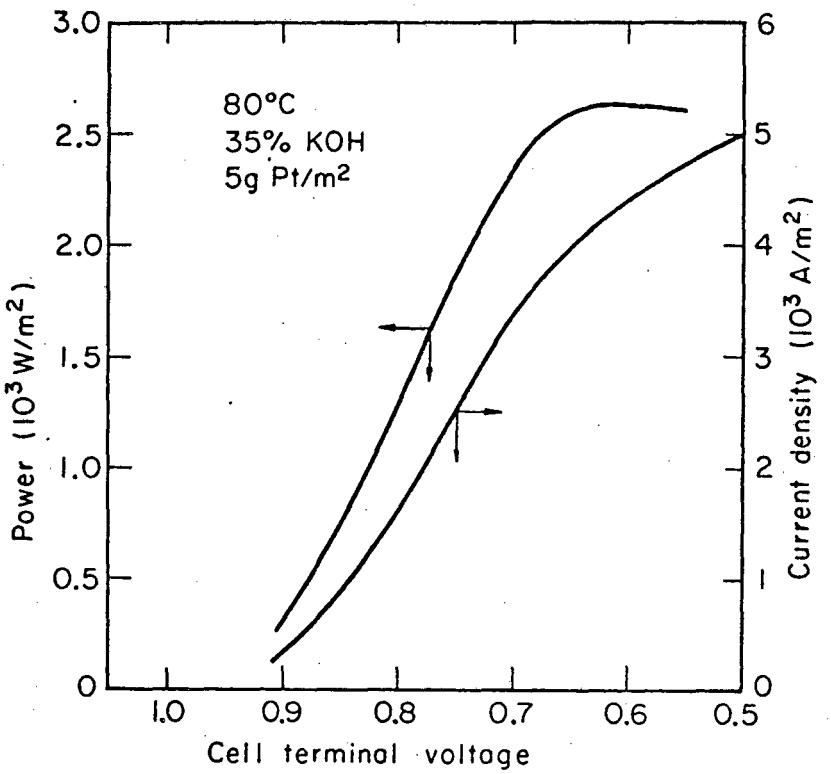

FIG. 6. PERFORMANCE CURVES FOR SINGLE 16 cm^2 CELL.

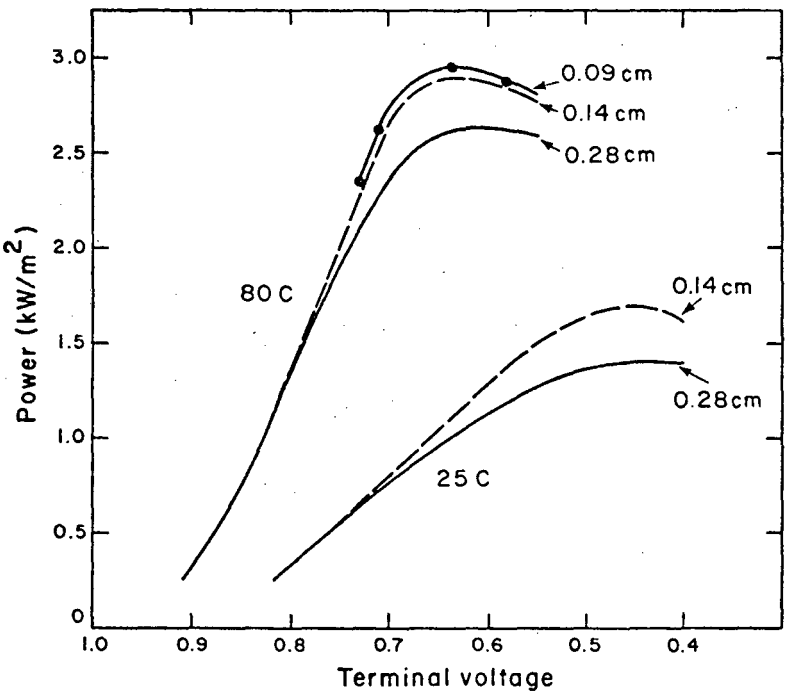

FIG. 7. EFFECT OF INTERELECTRODE GAP ON THE SINGLE CELL PERFORMANCE CURVES.

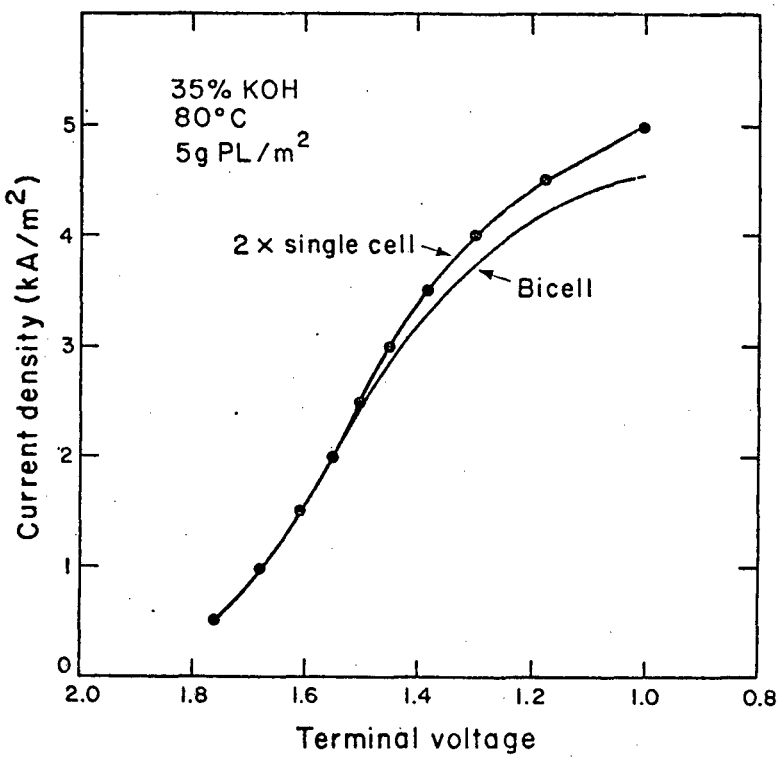

FIG. 8. COMPARISON OF THE OBSERVED POWER CURVE WITH 16 cm^2 BICELL TO THE EXPECTED CURVE (FROM SINGLE CELL DATA).

electrodes of 16 cm^2 active area. The conclusion from the laboratory studies was that the bipolar flowing electrolyte alkaline fuel cell concept presented here is practical and that power densities of 1 - 2.6 kW/m^2 at 0.7 - 0.8 V per cell are achievable with current technology.

The effect of unreacted ammonia was not determined in a definitive manner. At 80°C, there was a slight poisoning effect on the anode catalyst at high utilization at the 1.5% NH_3 level but even levels as high as 5% NH_3 did not have a deleterious effect on cell performance. At lower temperature, the effect of 1.5% NH_3 was complex, and depended on the temperature history of the cell. When the cell was cooled to room temperature with a pure hydrogen anode gas, switching to 1.5% NH_3 did not produce a significant effect in the first hour. The initial room temperature performance curve of the single cell is also shown in Fig. 7. The decrease in conductivity (factor of 3) makes the room temperature performance more sensitive to the interelectrode gap than at 80°C. After several hours the polarization of both anode and cathode increased dramatically, to the point where the power density dropped by over an order of magnitude. Switching back to pure hydrogen did not restore the initial room temperature performance even after several hours, but replacement of the electrolyte coupled with the switch to pure hydrogen resulted in rapid recovery. Apparently ammoniation of the electrolyte occurs at room temperature from prolonged exposure to the 1.5% NH_3 hydrogen stream and poisons both anode and cathode. Heating the cell back to 80°C restored the initial high temperature performance of the

cell, probably as a result of ammonia rejection from the cell at this temperature. In practical use, ammoniation of the electrolyte can be avoided, since the fuel cell would be cooled down to ambient temperature only when the system is not in use, at which time there is no ammonia going into the fuel cell. The conclusions from this study are, therefore, that unreacted ammonia at the 1.5% level has no effect on a hot fuel cell, but the system operation should be controlled such that when cold, as in a cold start condition, extended exposure to >1.5% ammonia does not occur.

ENGINEERING DESIGN OF COMPONENTS

For the purpose of comparing the NH_3-air fuel cell system concept to other advanced concepts for vehicle power sources, engineering design of the major components of the system was done to estimate the weight and volume of a power plant configured for a vehicle. The design was based on our laboratory data on the ammonia cracking, on the fuel cell performance, and on prior engineering studies of ammonia storage on vehicles. The design analysis is given below for each of the major sections of the system.

Ammonia Storage/Vaporizer Subsystem

The present design differs slightly from previous designs[15] in that *in vita* vaporization is used. Ammonia is vaporized within the storage tank with the heat of vaporization supplied by the waste heat from the fuel cell. In steady-state operation, the flowrate of hot electrolyte to the ammonia tank is regulated to maintain the liquid ammonia temperature at 25°C so that vapor is delivered to the cracker at 10 bar. The excess waste heat from the fuel cell is rejected to the ambient through a heat exchanger. The fuel tank weight was calculated with the assumptions of: a cylindrical shape with spherical ends; a maximum liquid ammonia temperature of 50°C; maximum pressure of 20 bar; fabrication from Aℓ alloy 6061-T6. The fuel tank weight is 43.6% of the weight of the fuel including the internal heat exchanger.

Ammonia Cracking Subsystem

To minimize weight and volume, the air pre-heater, ammonia cracker and the vent gas burner are incorporated into a single annular unit, as in previous designs of ammonia crackers and methanol reformers for fuel cells.[24] A schematic is shown in Fig. 9. As described in the previous section, the inverse order of the cracking kinetics in hydrogen pressure means that the reaction rate is highest at the front of the bed. Since it has been shown[25] that the minimum reactor volume results when the heat input is highest where the rate is highest, the burner gas flows are co-current, with the maximum ΔT at the bed entrance. The calculated adiabatic flame temperature from complete combustion of the *dehumidified* anode vent gas with stoichiometric air at 80% utilization of hydrogen is 1490°C. Since the annular design of the burner should minimize heat losses from the combustion, we have based the system design on the assumption that the actual flame temperature is at least 1450°C (ca. 5% heat loss).

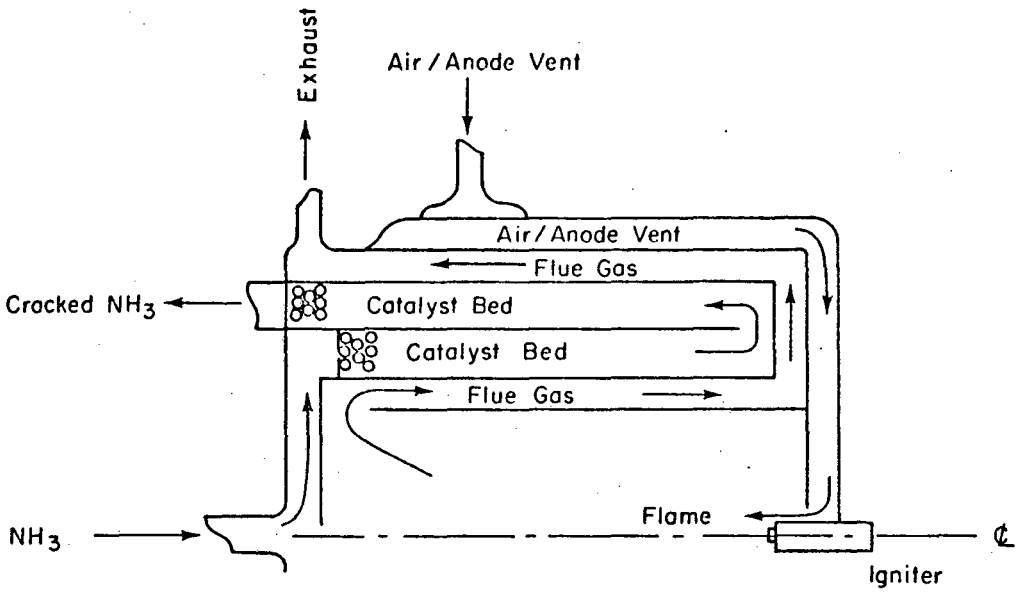

FIG. 9. SCHEMATIC DIAGRAM OF THE NH_3 CRACKER/BURNER UNIT WITH INTEGRAL COMBUSTION AIR PRE-HEATING.

The weight of the catalyst and the weight and volume of the subsystem depend on the gas throughput. According to Fig. 3, at the design conditions of 450°C and 10 bar, the amount of catalyst (in g) required to achieve equilibrium conversion is 17.66 Q (for Q in gmols NH_3 hr^{-1}). The ammonia throughput is related to the power from the cell and the voltage,

$$Q = 15.128 \left(\frac{P}{V}\right)$$

where P is the power delivered in kW and V is the volts per cell. The catalyst requirement is therefore

$$W_c(\text{in g}) = 267.1 \left(\frac{P}{V}\right)$$

The peak power for the alkaline cell occurs at about 0.65V (Fig. 8), so, for example, the catalyst required for 20 kW peak power would be 8.2 kg. For design purposes, the actual catalyst requirement was estimated to be twice this amount to allow for non-ideal operation, aging etc., or about 0.8 kg per kW of fuel cell peak power. The effective packed density of the catalyst in the bed is about 1.2 kg/ℓ, so the catalyst bed volume is about 0.7 ℓ/kW. The total preheater-cracker-burner subsystem volume is therefore 2.5 ℓ/kW and the weight, if fabricated from mild steel, 1.2 kg/kW for systems of 20-40 kW capacity. Very much smaller systems or very much larger systems would have different scaling factors.

Alkaline Fuel Cell System

The cell design is based on the repeating hardward of the laboratory bicell shown in Figs. 4 and 5. The repeating hardware is stacked in the

usual filter-press arrangement between copper endplates in the manner depicted in Fig. 5. The gas manifolds are at the ends of the stack and the liquid manifold in the side. For the scale-up from the laboratory 16 cm^2 cell, we assumed the internal manifold sealing area was 20% of the active area, e.g. a 20 cm x 20 cm active area (400 cm^2) would have a 1 cm sealing strip on the perimeter. The design was based on a 20 kW rated power cell delivered at a nominal voltage of 100 V. The fuel cell size required was calculated using the observed laboratory performance curve for the single cell but assuming a reduced separator thickness of 0.14 cm (vs. 0.28 cm). The repeating unit cell (1 bipolar plate, 1 separator, 2 electrodes) dimension was assumed to be 0.58 cm. The effective density of the unit cell filled with 35% KOH is 1.41 kg/ℓ. The relation between fuel cell size and the voltage efficiency is summarized in Table 3. The weights shown are exclusive of gas manifolds, endplates and tierod weights. Higher efficiency at the rated power is achieved at the expense of increased weight, volume, and total materials costs for the cell. As in any fuel cell system, the optimum cell design depends on economic factors related to amortization of the capitol, cost of fuel, use factors, etc. For the purposes of evaluating both the economic factors and the vehicle performance, it is essential to have the parametric relations between efficiency and size and the data in Table 3 are sufficient to establish these relations. One of the important parameters for vehicle simulation not in Table 3 is the cell stack peak power. The "peak" power shown in Fig. 9 is a steady-state value representing the maximum sustained power that can be produced. If we consider peak power as the power available in a transient from low load to high load, the result is a "peak" power that is anywhere from 1 to 5 times the maximum power, depending on the duration of the peak load. Since there are a number of transport processes that contribute to the polarization at high load, the characteristic times for current transients are those for the depletion of diffusion layers (liquid, gas-pore, gas-film, etc.) generally a few seconds or even less. For practical purposes, such as vehicle acceleration, the duration of peak loads may be tens of seconds, so that the cell stack cannot produce peak power much greater (<10%) than the maximum sustained power. The useful peak power density of the bipolar stacks in Table 3 is, therefore, 270 W/kg, exclusive of the weight of the auxiliary systems (manifolds, process air blower, coolant pumps, plumbing, etc.).

The weights and volumes of the three major components of the system can be estimated from the engineering design with reasonable accuracy. The supporting apparatus, (e.g. the electrolyte coolant subsystem, the process air blower and manifold, the structure to hold everything together, etc.) weight and volume is more difficult to estimate since a prototype of this system has not actually been built. The approach used here to develop an estimate of the supporting apparatus was to use the estimates for similar components in the advanced phosphoric acid fuel cell made by United Technologies.[27] That power plant was also liquid cooled and the component analysis was made based on about the same voltage efficiency (ca. 0.75V per cell) as that used here, so the heat load on the coolant system is about the same. The process air gas flows would also be of similar magnitude, so the process air blower and plenum would be of comparable size. Using these rather rough guidelines, the estimated weight and volume for a fuel cell system with 20 kW rated (continuous) power

and 50 kW peak power is shown in Table 4, exclusive of the weight of ammonia or the ammonia storage tank. The cell configuration used in Table 4 provided the highest peak power density consistent with reasonable projected cost. As is clear from Table 4, the fuel delivery subsystem and the auxiliary components reduce the fuel cell peak power by a factor of two, i.e. the cell stack itself is about 50% of the weight of the total system.

TABLE 3. RELATION BETWEEN VOLTAGE EFFICIENCY AND CELL STACK SIZE FOR 20 kW CONTINUOUS POWER.

V (V per cell)	Power (kW/m^2)	N	A (m^2)	Ae (cm^2)	Wgt. (kg)	Vol. (ℓ)
.65	2.60	155	9.3	500	76	54
.70	2.35	143	10.2	595	83	59
.75	1.80	133	13.3	835	109	77
.80	1.30	125	18.4	1230	151	107
.825	1.05	121	22.8	1570	186	132

TABLE 4. ESTIMATED COMPONENT SIZES FOR A 20 kW CONTINUOUS- 50 kW PEAK POWER NH_3-AIR FUEL CELL SYSTEM.

Cell configuration: 100V (.825 V/cell) @ 200A continuous
80V (.65 V/cell) @ 636A peak

1.)	Cell stack	186 kg	132 ℓ
2.)	NH_3 Cracker/Burner	60	125
3.)	NH_3 Pre-heater	10	8
4.)	Hydrogen Plenum	10	6
5.)	Process Air Blower and Plenum	20	10
6.)	Anode Gas Dryer	1	0.3
7.)	Coolant Loop		
	a.) Scrubber + KOH	10	7
	b.) Pump and motor (100W)	20	0.8
	c.) Waste heat radiator	2	0.6
8.)	Structure, Plumbing, Valves	35	-
	Total	354 kg	290 ℓ
	Peak Power Density	141 W/kg	172 W/ℓ

Fuel efficiency at 20 kW continuous 3.032 kWh/kg NH_3 or 1.819 kWh/ℓ NH_3.

For comparison of the NH_3 storage concept with other hydrogen storage concepts, it is of interest to report separately the weights for the ammonia tank and the ammonia cracking components. For a 50 kW peak power - 80 kWh system, which would give a passenger vehicle range of ca. 500 km, the ammonia weight would be 33 kg, the tank 12 kg, the ammonia pre-heater 10 kg and ammonia cracker-burner unit 60 kg, or a total hydrogen supply system weight of 115 kg containing 5.8 kg of hydrogen. The NH_3 system as designed here stores hydrogen at 5.1 w/o, which is about 6 times higher than the hydride system used in the previous LASL hydride-alkaline fuel cell vehicle simulation.[14]

SYSTEM CHARACTERISTICS

The output characteristics of the total ammonia-air fuel cell system can be calculated from Table 3 and equations [3] and [4] and the estimated weights and volumes of all components. For the purposes of comparison with systems using different fuels, the characteristics of the system should be given in terms of power density inclusive of the ammonia weight (and volume) and the weight of the ammonia storage tank, i.e. the specific power- specific energy relation (the Ragone Curve). This relation was calculated from the weight of the components for the 20 kW continuous -50 kW peak configuration plus the ammonia weight and the storage tank weight for 40-160 kWh, then normalizing the power and energy delivered by the total weight. The Ragone Curve for the ammonia-air fuel cell is shown in Fig. 10 compared to the projected plots for methanol and gasoline fueled ICEs in the 1990-2000 timeframe (from Ref. 20). The power density falls short of that for the methanol-ICE but is greater than the specific power recommended for adequate acceleration of battery powered vehicles. Moreover, the ammonia-air system delivers continuous power at 62.8% efficiency, more than twice full-throttle efficiency of a methanol-ICE. It appears at least feasible for the ammonia-air bipolar alkaline fuel cell system, described in this work, to meet the minimum acceleration requirements for advanced vehicles with the appropriate engineering development. The attractiveness of the system relative to other advanced vehicle concepts would be enhanced by improving the peak power to full equivalence with methanol-ICE (factor of two). Since the weight of the cell stack is only 50% of the total system weight, the cell stack power density would have to be increased by a factor of four to reach equivalence. Such a large increase relative to the technology in Fig. 6 could only be achieved by a remarkable breakthrough in both electrode technology (to reduce transport losses) and electrocatalysis (anodic shift of the entire curve). Alternatively, the present technology could be used in a hybrid vehicle with batteries specifically designed for high current short-duration discharge and low current extended charge. In this type of system the specific power of the fuel cell is less critical and there are a number of design options. More specifically, one needs to examine the tradeoff between fuel cell efficiency, fuel cell weight, vehicle weight, and vehicle fuel consumption over a driving cycle to determine which of the fuel cell configurations in Table 3 is the optimum for a hybrid system. The tradeoffs can be examined by computer simulation using the relation between fuel cell efficiency and continuous power density shown in Table 5. The entries

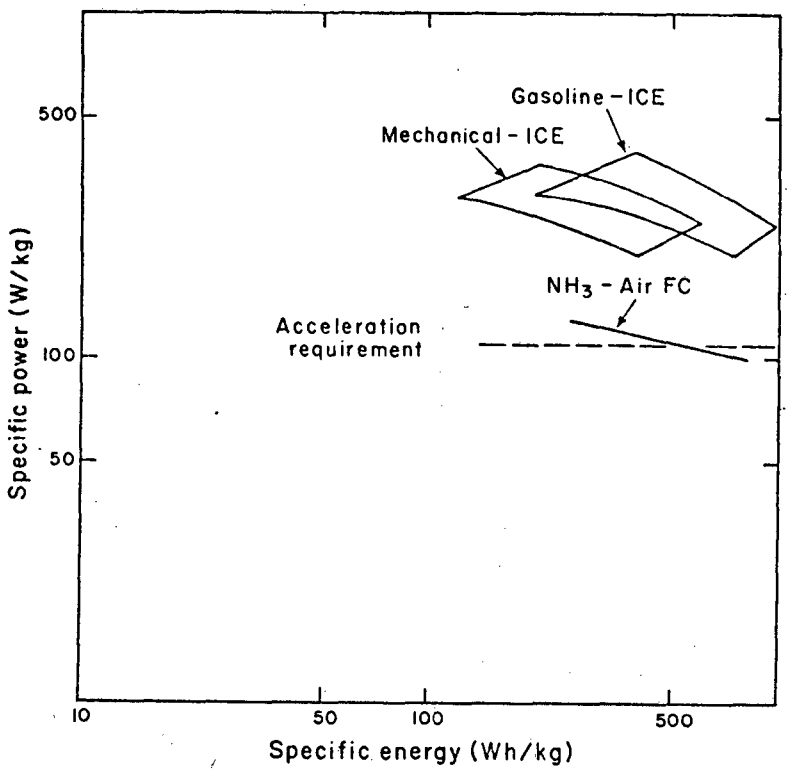

FIG. 10. RAGONE PLOT FOR THE NH_3-AIR FUEL CELL POWERED VEHICLE RELATIVE TO THE PROJECTIONS FOR METHANOL-ICE POWERED VEHICLE.

in Table 5 were calculated from Tables 3 and 4 and equations [5] and [6], with modification to the component weights and volumes in Table 4 to reflect only continuous 20 kW power. The design option is the current density at which continuous power is delivered by the cell stack; increasing current density results in the usual tradeoff between efficiency and size. Size impacts both weight (volume) and materials cost of the cell stack, so there is a further economic tradeoff to be examined between initial cost of the system and the fuel savings over the lifetime of the device. These complex tradeoffs require extensive computer simulation to select the optimum configuration of the fuel cell for a given type of peaking battery and a given fuel cost scenario.

Since a complete system like that described here has never been built, and there are as yet no established manufacturing costs for fuel cell type components, detailed economic analysis is premature. However, as a benchmark, one can make an accurate estimate of the materials cost, based both on the present piece-part cost and the projected cost for high volume production, as done in Table 6. The piece-part cost is defined as the cost to LBL at the time of purchase, and the projected price represents either large volume (e.g. the carbon paper) cost or a less expensive manufacturing process cost (e.g. the bipolar plates). The graphite bipolar plate is the most expensive single constituent in the cell stack, and there are many active programs in the phosphoric acid fuel cell field directed at lowering the cost of bipolar plates. The bipolar alkaline fuel cell may benefit from the development of new low-cost bipolar plate

TABLE 5. THE RELATION BETWEEN FUEL EFFICIENCY AND CONTINUOUS POWER DENSITY FOR THE AMMONIA-AIR FUEL CELL SYSTEM

Design option (kA/m^2)	Thermal Eff. (%LHV)	Fuel Eff. (kWh/kg)	Power (W/kg)	Density (W/ℓ)†
4	49.5	2.389	101	76
3.4	53.3	2.573	98	73
2.4	57.1	2.757	87	65
1.6	60.9	2.940	73	55
1.3	62.8	3.032	65	49

†50% packing factor.

TABLE 6. MATERIALS COST FOR THE BIPOLAR ALKALINE FUEL CELL STACK.

Material	Cost (1982) per m^2	
	Present	Projected
Pt Catalyst	$50	$20[a]
Carbon paper	$43	$27[b]
Polypropylene	$ 4	$ 4
Graphite sheet	$75	$35[c]
Teflon	$28	$28
	$200	$114

[a] Non-Pt catalyst at air electrode

[b] Economy of scale

[c] Cost of materials for direct fabrication from graphite powder and resin into a graphite composite.

materials in these programs, although the stability requirements for 35% KOH at 70°C may be different than for 98% H_3PO_4 at 180°C. The elimination of Pt catalyst at the air electrode and the substitution of an inexpensive material at equivalent performance would lower the projected materials cost to about $100 m^{-2}. The projected materials cost for the

20 kW-continuous-50 kW peak cell stack in Table 4 would therefore be about $2200 or about $40 per peak kW, which seems like a very competitive figure. The 20 kW continuous power fuel cells in Table 3 have projected cell stack materials cost of $800 to $2000, depending on the design option selected. The materials cost of the total cell system would be more, as the cost of the auxilliary systems must be added in, but these materials are relatively inexpensive. Since there are a number of batteries that have materials cost less than $20 per peak kW and peak power densities significantly greater than 100 W/kg, the economic and performance advantages of a battery hybrid system make this type of system look even more attractive. Initial cost consideration favors the selection of the high current density option in Table 5 for a hybrid power plant, but fuel costs over the life of the system favor the lower current density configuration. The increase in weight of the power plant with the increase in thermal efficiency tends to reduce the actual gain in fuel consumption, so a computer simulation of expected fuel consumption as a function of cell configuration is required for quantitative evaluation of the options in Table 5.

CONCLUSIONS

1. A hydrogen-air bipolar, flowing electrolyte alkaline fuel cell with 2.6-3.0 kW/m^2 peak power has been demonstrated using currently available materials and technology.

2. An ammonia cracker can be thermally integrated with a low temperature alkaline fuel cell and maintain high (>50% of LHV of NH_3) overall conversion of NH_3 to electrical energy.

3. On-board storage of hydrogen as liquid ammonia and recovery of the hydrogen content by catalytic cracking results in a hydrogen storage system containing about 5 w/o hydrogen, which is 2.5-6 times higher than metal hydride systems.

4. The 20 kW Continuous - 50 kW Peak Power NH_3-air alkaline fuel cell system designed here has a peak power density of 141 W/kg (172 W/ℓ) and a continuous fuel efficiency of 3.032 kWh/kg NH_3 (62.8% LHV of NH_3).

5. The projected materials cost of the fuel cell system is $40-50 per peak kW.

6. Lower power system cost would probably result if a battery-fuel cell hybrid system were developed, as the fuel cell is probably a more expensive way of adding peak power to the system.

ACKNOWLEDGMENTS

The author acknowledges valuable discussions with Dr. N. Spencer of W. R. Grace on ammonia catalysis and with Mr. David Bloomfield of Physical Sciences Inc. on fuel cell systems integration. This work was supported by the Assistant Secretary for Conservation and Renewable Energy, Office

of Advanced Conservation Technology, Electrochemical System Research Division of U.S. Department of Energy, under Contract DE-AC03-76SF00098.

REFERENCES

1. P. Ross, in Proceedings of the Symposium on Electrocatalysis, eds. W. O'Grady, P. Ross and F. Will, The Electrochemical Society, PV 82-2, pp 24-39.
2. E. Yeager and P. Bindra, DOE Battery and Electrochemical Contractor's Conference, Arlington, VA, December 1979.
3. P. Ross and F. Wagner, Lawrence Berkeley Laboratory Report UCRL-14192, May 1982.
4. L. Handley, A. Meyer, and W. Bell, Pratt and Whitney Aircraft Report to NASA, #CR-134721, January 1975.
5. K. Kordesch, J. Electrochem. Soc., 125, 77C (1978).
6. EXXON Enterprises, Final Report to EPRI, EM-384 (RP 584-1), January 1977.
7. K. Kordesch, 4th World Hydrogen Energy Conference, Pasadena, CA, June 1982.
8. K. Kordesch, "Survey of Carbon and its Role in Phosphoric Acid Fuel Cells," Brookhaven National Laboratory Report BNL-51418, December 1979.
9. J. Reilly and G. Sandrock, Sci. Amer., 242, 118 (1980); K. Hoffman, J. Reilly, F. Salzano, C. Warde, R. Wiswall and W. Winsche, Fuels and Lubricants Meeting of the Society of Automotive Engineers, St. Louis, Missouri, June 7-10, 1976.
10. H. Buchner, Prog. Energy Combust. Sci., 6, 331 (1980).
11. W. Escher, "Survey of Liquid Hydrogen Container Techniques for Highway Vehicle Final System Applications," U.S. DOE Report HCP/M2752-01, November 1978.
12. J. Swisher and E. Johnson, J. Less-Comm. Met., 74, 301 (1980).
13. R. Teital, "Microcavity Hydrogen Storage," Brookhaven National Lab Report BNL-51439.
14. D. Lynn, "Analysis of Vehicle Systems Using Hydrogen Storage/Alkaline Fuel Cell Technology," Los Alamos Scientific Lab Report LA-VR-80-3094.
15. E. Behrin, et al., "Energy Storage System for Automatic Propulsion," Volume 2, December 1977, LLNL Report UCRL-52303 Volume 2, pp 136-141, 276.
16. E. Simons, D. McKee and E. Cairns, Proceedings of the Third Int. Symp. on Fuel Cells, Brussels, 1969, pp 131-38.
17. P. Ross and V. Kopytov, to be published.
18. A. Larson and B. Dodge, J. Amer. Chem. Soc., 45, 2918 (1923).
19. E. Cairns and D. Macdonald, J. Electrochem. Soc., Electrochem. Tech., 2, 65 (1964).
20. L. O'Connell, et al., "Energy Storage Systems for Automobile Propulsion," Volume 3, December 1980, LLNL Report UCRL-53053-80, Vol. 3, pg 5-7.
21. P. Emmett, in "The Physical Basis for Heterogeneous Catalysis," eds. E. Drauglis and R. Jaffe, Plenum, 1975, p 3ff.
22. P. Ross, EPRI Final Report on Project 1200-5, EPRI EM-1553, September 1980.

23. W. Dyson, et al., J. Electrochem. Soc., 115, 566 (1968).
24. M. Collins, R. Michalek, and W. Brink, Proc. 7th Int. Energy Conv. Engr. Conf., San Diego, CA, 1972, pp 32-36.
25. K. Denbigh, "Chemical Reactor Theory," Cambridge University Press, 1965, pp 132-141.
26. F. Rossini, et al., Selected Values of Chemical Thermodynamic Properties, NBS Circular No. 500, U.S. Gov. Printing Office, 1952; see also L. Haar and J. Gallagher, J. Phys. Chem. Ref. Data, 1, 635 (1978) for the latest compilation of the thermodynamic properties of ammonia.
27. United Technologies Corporation, Report to Los Alamos Scientific Laboratory, FCR-4059, May 1982.

This report was done with support from the Department of Energy. Any conclusions or opinions expressed in this report represent solely those of the author(s) and not necessarily those of The Regents of the University of California, the Lawrence Berkeley Laboratory or the Department of Energy.

Reference to a company or product name does not imply approval or recommendation of the product by the University of California or the U.S. Department of Energy to the exclusion of others that may be suitable.

TECHNICAL INFORMATION DEPARTMENT
LAWRENCE BERKELEY LABORATORY
UNIVERSITY OF CALIFORNIA
BERKELEY, CALIFORNIA 94720